

The coalescence and strength of rock-like materials containing two aligned X-type flaws under uniaxial compression

Bo Zhang^{*1}, Shucaï Li^{2a}, Xueying Yang^{3b}, Kaiwen Xia^{4c}, Jiyang Liu^{1d}, Shuai Guo^{1e} and Shugang Wang^{2f}

¹School of Civil Engineering, Shandong University, Jinan, Shandong 250061, P.R. China

²Research Center of Geotechnical and Structural Engineering, Shandong University, Jinan, Shandong 250061, P.R. China

³Shandong Urban Construction Vocational College, Jinan, Shandong 250014, P.R. China

⁴Impact and Fracture Laboratory, Department of Civil Engineering and Lassonde Institute, University of Toronto, ON M5S 1A4, Canada

(Received January 20, 2018, Revised November 28, 2018, Accepted December 10, 2018)

Abstract. Crossing (X-type) flaws are commonly encountered in rock mass. However, the crack coalescence and failure mechanisms of rock mass with X-type flaws remain unclear. In this study, we investigate the compressive failure process of rock-like specimens containing two X-type flaws aligned in the loading direction. For comparison purposes, compressive failure behavior of specimens containing two aligned single flaws is also studied. By examining the crack coalescence behavior, two characteristics for the aligned X-type flaws under uniaxial compression are revealed. The flaws tend to coalesce by cracks emanating from flaw tips along a potential path that is parallel to the maximum compressive stress direction. The flaws are more likely to coalesce along the coalescence path linked by flaw tips with greater maximum circumferential stress if there are several potential coalescence paths almost parallel to the maximum compressive stress direction. In addition, we find that some of the specimens containing two aligned X-type flaws exhibit higher strengths than that of the specimens containing two single parallel flaws. The two underlying reasons that may influence the strengths of specimens containing two aligned X-type flaws are the values of flaw tips maximum circumferential stresses and maximum shear stresses, as well as the shear crack propagation tendencies of some secondary flaws. The research reported here provides increased understanding of the fundamental nature of rock/rock-like material failure in uniaxial compression.

Keywords: aligned X-type flaws; rock-like material; crack coalescence; strength; uniaxial compression

1. Introduction

Underground structures such as tunnels, mines, caverns, and storage facilities have been and are being developed and constructed around the world (Li *et al.* 2016). It is thus of great importance to understand the failure process of rock materials to ensure these structures to be safely designed and constructed. However, it is a challenging task to investigate the rock failure process because of the brittleness of the rock material and the embedded flaws.

Rock failure process usually can be divided into three

stages, namely crack initiation, propagation, and ultimate failure (Park and Bobet 2010). In the early 20th century, Griffith (1921) began to study the crack initiation and propagation in brittle material such as glass. After that, some researchers began to investigate the rock failure process. Hoek and Bieniawski (1965) examined the crack initiation and propagation in rock specimens containing a single flaw under compression (hereafter the term “flaw” will be used for pre-existing cracks, while the term “crack” is used for new fracture generated due to loading). After that more failure processes have been investigated in the rock material containing a single inclined flaw (Huang *et al.* 1990, Al-Shayea 2005), such as using gypsum or cement mortar (Lajtai 1974, Sahouryeh *et al.* 2002, Wong and Einstein 2009). Feng *et al.* (2017) studied the mechanical behaviors of fissured specimens under coupled static and dynamic loads with different loading parameters. Liu and Dai (2018) established a damage constitutive model with a definite physical significance for intermittent jointed rocks under cyclic uniaxial compression. From the results on failure processes in rock/rock-like materials containing a single flaw, some conclusions have been reached. Specifically, there are two types of cracks occurred under uniaxial compression test condition: the wing crack and the secondary crack. The wing crack is tensile crack and the secondary crack is shear crack.

The rock/rock-like material specimens containing a single flaw under compression could only be used to study

*Corresponding author, Associate Professor

E-mail: zhangbo1977@sdu.edu.cn

^aProfessor

E-mail: lishucaï@sdu.edu.cn

^bLecturer

E-mail: 274679821@qq.com

^cProfessor

E-mail: kaiwen.xia@utoronto.ca

^dM.Sc. Candidate

E-mail: 961491834@qq.com

^eM.Sc. Candidate

E-mail: 569294235@qq.com

^fProfessor

E-mail: shugangwang@gmail.com

the crack initiation and ultimate failure modes. These tests could not be used to explain the crack coalescence process and mechanism behind. In order to further explore the rock failure process, researchers started to study the failure process of rock/rock-like materials containing two flaws.

Shen *et al.* (1995) studied the crack coalescence with rock-like material specimens containing two flaws under uniaxial compression. From their experimental results they proposed two coalescence modes: (1) the pre-existing flaws coalesce through tensile cracks when they overlap, (2) the coalescence occurs through shear cracks when the pre-existing flaws do not overlap. Bobet and Einstein (1998), Wong and Chau (1998) investigated crack coalescence with rock-like material specimens containing two pre-existing parallel flaws in uniaxial and biaxial compression. Their research results showed that there are three types of crack coalescence modes during compression: shear mode, tensile mode and mixed shear/tensile mode. Bobet (2000) studied the initiation of secondary cracks under compression with rock-like materials containing two parallel flaws. He proposed an extension of the maximum shear stress criterion to predict the initiation of secondary cracks. Li *et al.* (2005), Wong and Einstein (2009), Yang (2011), Chen *et al.* (2012) and Yin *et al.* (2014) experimentally explored the failure processes of rock specimens containing two parallel flaws under compression. Haeri *et al.* (2014) experimentally studied the failure processes of rock specimens with Brazilian disks containing double non-parallel flaws under compression. Their results indicated that the orientations and geometries of flaws could affect the failure process of the specimens.

In most field cases the flaw pattern in rock mass would be in the form of multi-flaws. Therefore it is desirable to study the failure process in specimens with parallel multi-flaws. Wong *et al.* (2001) and Cao *et al.* (2015) analyzed the crack coalescence in rock-like material containing three parallel flaws using experimental approaches. Sagong and Bobet (2002) investigated coalescence in rock-like material containing three and sixteen flaws under uniaxial compression. Park and Bobet (2009) conducted crack coalescence tests with specimens containing two, three and sixteen parallel flaws loaded under uniaxial compression. Sagong *et al.* (2011) analyzed the failure process of an opening in a jointed rock mass containing ten parallel flaws under biaxial compression. Pu and Cao (2012) studied the failure process of rock-like material specimens containing fifteen, twenty, twenty-five and thirty parallel flaws under uniaxial compression. Zhou *et al.* (2014) experimentally examined the crack coalescence in rock-like material under uniaxial compression with specimens containing four parallel flaws. Liu *et al.* (2017a) studied the failure process of rock-like material specimens containing three, six, nine, twelve and fifteen parallel flaws under cyclic uniaxial compression. Liu *et al.* (2017b) studied the fatigue mechanical properties of synthetic jointed rock models under different cyclic conditions. The results show that when the loading frequency is low or the maximum stress and amplitude are high, samples have higher fatigue deformation modulus and lower fatigue life. Cheng *et al.* (2016) analyzed the crack openings influence the mechanical and cracking behavior of the specimens containing three pre-existing flaws. Zhou *et al.* (2018)



Fig. 1 Rock mass containing X-type flaws

studied the effects of brittleness and rock bridge angle on crack initiation, propagation and coalescence mechanism in the rock-like specimens containing three preexisting flaws under uniaxial compression. In their works four types of crack initiation patterns and ten types of coalescence patterns were observed and presented.

As far as numerical methods, many researchers have investigated crack propagation and flaw tip stress fields. Some conducted numerical simulations with the Rock Failure Process Analysis code (RFPA) (Tang *et al.* 2001). ABAQUS is also an effective FEM approach to explore flaw tip stress and fracture process (Wei *et al.* 2016). The discrete element method (DEM) and the extended finite element method (XFEM) are also used extensively (Sharafisafa and Nazem 2014, Liu *et al.* 2017c). There are also many other numerical approaches used by scholars in modelling the crack initiation, propagation and coalescence in fractured rock mass (Li *et al.* 2016).

All the results discussed above show that the geometry of the flaws has a great influence on the failure process of rock/rock-like material. Up to now the flaws in rock/rock-like specimens studied are mostly single flaw or parallel multi-flaws. In the real rock mass there are a great number of X-type flaws (Fig. 1). It is thus crucial to understand how the X-type flaws influence the rock failure process and strength. However, there are very limited studies on X-type flaws in literatures (Zhang *et al.* 2016). This study thus aims at understanding the crack coalescence and ultimate failure mechanism of rock-like material containing two aligned X-type flaws under uniaxial compression testing condition. The experimental results of specimens containing two aligned X-type flaws have been compared with those of specimens containing two single flaws.

We will introduce specimen preparation and testing equipment in Section 2. The experiments and numerical results including the crack coalescence characteristics and the peak strength of specimens containing two aligned X-type flaws under uniaxial compression are then analyzed and discussed in Section 3, followed by some conclusions made in Section 4.

2. Specimen preparation and testing equipment

2.1 Specimen design

For comparison purpose, two types of flaws were considered in this study, i.e., two parallel single flaws and

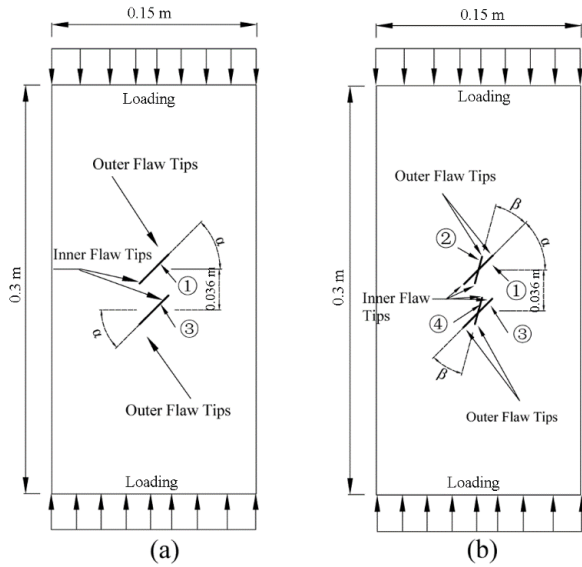


Fig. 2 The schematics of specimens containing different type of flaws: (a) the specimen containing two single flaws and (b) the specimen containing two aligned X-type flaws

Table 1 Testing Conditions of rock-like materials containing two aligned X-type flaws under uniaxial compression

| No. | $L13(m)$ | $L24(m)$ | $\alpha(^{\circ})$ | $\beta(^{\circ})$ |
|-----|-----------------------------|----------|--------------------|-------------------|
| C1 | 0.03 | N/A | | N/A |
| C2 | 0.03 | 0.02 | | 15 |
| C3 | 0.03 | 0.02 | | 30 |
| C4 | 0.03 | 0.02 | | 45 |
| C5 | 0.03 | 0.02 | | 60 |
| C6 | 0.03 | 0.02 | | 75 |
| C7 | 0.03 | 0.02 | 45 | 90 |
| C8 | 0.03 | 0.02 | | 105 |
| C9 | 0.03 | 0.02 | | 120 |
| C10 | 0.03 | 0.02 | | 135 |
| C11 | 0.03 | 0.02 | | 150 |
| C12 | 0.03 | 0.02 | | 165 |
| C13 | specimens without any flaws | | | |

Note: $L13$ - the length of primary flaws ① and ③; $L24$ - the length of secondary flaws ② and ④

two aligned X-type flaws, (denoted by flaws Type I and II, respectively) as shown in Fig.2. The two individual flaws in the flaw Type I are labeled as ① and ③, respectively (Fig. 2(a)). The four individual flaws in the flaw Type II are labeled as ①, ②, ③ and ④, respectively (Fig. 2(b)). In all specimens, flaws ① and ③ are in parallel and called the primary flaws with a length of 0.03 m, whereas flaws ② and ④ are in parallel and called the secondary flaws with a length of 0.02 m. In Fig.2, α represents the angle between the primary flaws (i.e. flaws ① or ③) and the



Fig. 3 A typical specimen containing two aligned X-type flaws



Fig. 4 The testing apparatus

horizontal direction and it is fixed at 45° . β denotes the angle between the primary and secondary flaws, and β varies from 15° to 165° with an increments of 15° . The distance between the two crossing points of the two aligned X-type flaws is 0.036 m. The flaw tips are called the inner and outer tips as illustrated in Fig. 2.

The testing conditions of rock-like materials containing two aligned X-type flaws under uniaxial compression are listed in Table 1. In Table 1 the testing condition C1 without β is the specimen containing two single flaws. The testing condition C13 does not have any flaws. In Fig.2 and Table 1 the anticlockwise direction is described as the positive direction of angles α and β .

2.2 Specimen preparation

In this study, the rock-like material specimens were used to investigate the failure process. The specimens are casted in the steel mold using the cement mortar, which is made of #325 Portland cement and sand with the maximum diameter of 1.25 mm. The mixture ratio design of cement mortar is 1:5.09:0.96 for cement, sand and water, respectively. Two types of flaws are considered in this study, namely two parallel single flaws and two aligned X-type flaws. Flaws were created by inserting steel shims with 0.3 mm thickness in the mortar during casting and then removing them during curing. These flaws can be considered as open flaws.

In this study, three specimens for one testing condition were cast and tested. If the pattern of crack coalescence of at least two specimens in one testing condition is the same,

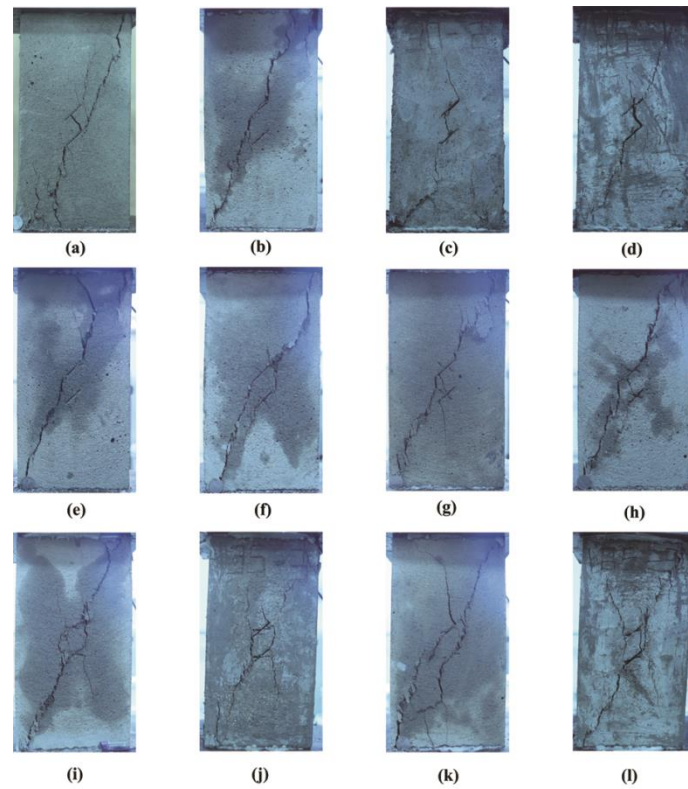


Fig. 5 Coalescence and failure modes of rock-like specimens containing two aligned X-type flaws under uniaxial compression. (a)-(l) denote testing conditions from C1 to C12, respectively

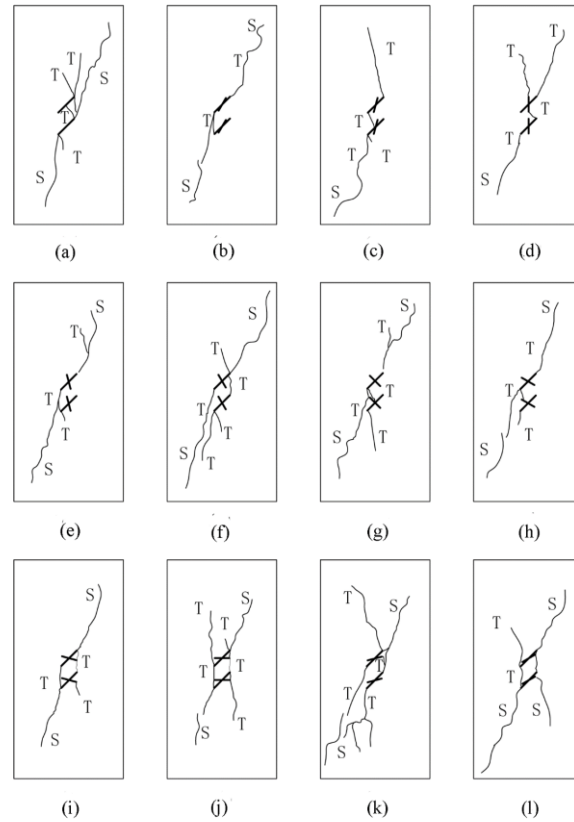


Fig. 6 Coalescence and failure modes schematic diagram of specimens containing two aligned X-type flaws under uniaxial compression. "T" and "S" denote tensile and shear cracks respectively. (a)-(l) denote testing conditions from C1 to C12, respectively

it will be taken as the crack coalescence pattern for this testing condition. If there is no repetitive coalescence pattern in three specimens, more tests should be conducted for this testing condition. If the maximum strength of the three specimens is not greater than 1.05 times of the average strength and the minimum strength of the three specimens is not smaller than 0.95 times of the average strength, the mean value of the three specimens' peak strengths is taken as the strength for this testing condition. Otherwise more specimens should be reconstructed and retested under this testing condition.

The specimen is a prismatic block with a length, width and height of 0.15 m, 0.15 m and 0.3 m, respectively. The flaws are made through the thickness of the specimen, perpendicular to the $0.15 \times 0.3 \text{ m}^2$ face.

The procedures to make specimens are described as follows. First, the sand is poured into a screen to remove particles larger than 1.25 mm. Then the cement, sand and water are mixed with the designed mixture ratio and blended for 5 minutes. The mixture is poured into the steel mold and is vibrated at room temperature for 3 minutes. The pre-existing flaws position is marked at the surface of the cement mortar with half an hour curing before inserting steel shims into the mortar. Then the steel shim is inserted into the cement mortar against a block with 10 cm thickness to assure the vertical direction of the inserting steel shim. The steel shim is removed from the cement mortar along the block 3 hours later. Finally, the specimens are cured at a constant temperature of 20°C and a constant humidity for 28 days. One of the cured specimens is shown in Fig. 3.

2.3 Testing apparatus

The testing apparatus is a servo control loading frame (Fig. 4), with a maximum capacity of 300 kN. The displacement control method was used to apply the load on the specimen with a loading rate of 0.5 mm/min. The specimens were loaded in a uniaxial compression condition until failure. The loading direction is parallel to the longitudinal direction of the specimen.

3. Experimental results and discussions

Testing results show that the failure process of rock-like material containing two aligned X-type flaws includes crack initiation, crack coalescence and final failure. A video camera was used to capture the failure process of specimen during the whole loading process. The strain-stress curve was recorded automatically by the acquisition system in the testing facility. The detailed observations and results are described below.

3.1 Crack coalescence of rock-like material specimens containing two aligned X-type flaws under uniaxial compression

The coalescence is the linkage of two cracks at the rock bridge. The cracks' coalescence modes are shown in Figs.5 and 6. The surfaces of tensile cracks and shear cracks have different characteristics. The surface of tensile cracks is characterized by a plumose structure and by the absence of

pulverized powder. The surface of shear cracks is characterized by pulverized material and a very rough texture, and it contains crushed material (Park and Bobet 2010). Based on this rule the cracks generated in the testing process are divided into tensile cracks and shear cracks, which are plotted in Fig. 6 and denoted with "T" and "S", respectively.

Shen *et al.* (1995) concluded that the pre-existing parallel single flaws coalesce through tensile cracks when they overlap. In our work the two aligned X-type flaws are overlapped, from Figs. 5 and 6 one can see that all the coalescence in specimens with two aligned X-type flaws occurred through tensile cracks as well.

From Figs. 5 and 6 it can be seen that there are different "T" and "S" cracks at the coalescence and failure modes in different specimens. From literatures (Bobet and Einstein 1998, Park and Bobet 2009) it can be known that there are stable and unstable propagation stages of "T" cracks. There is "S" crack at the failure of rock/rock-like material under uniaxial compression. The "T" cracks propagate towards the maximum principle stress. The "T" cracks propagation may delay the appearance of "S" crack. So the more the "T" cracks propagate, the higher the strength of specimens containing two aligned X-type flaws under uniaxial compression.

To get a deep insight into the crack coalescence, the finite element analysis (FEA) was used to simulate the stress field of specimens under uniaxial compression. The FEA model was developed using the software ABAQUS. The material parameters were used as $E = 1000 \text{ MPa}$ and $\nu = 0.25$, where E is the elastic modulus and ν is the Poisson ratio of the testing specimens. The values of E and ν were tested with specimens without any flaws under uniaxial compression (C13). The 6-node quadratic plane triangle elements (CPS6) were used around the flaw tip. 8-node biquadratic plane quadrilateral elements were used at the place except the areas around the flaw tips. As the flaw studied in this work was open flaw, the contacts between the flaw internal faces was not taken into consideration. The computation model and circumferential stress (σ_θ) field of specimen C5 are shown in Fig. 7 as an example. The γ in Fig. 7 is the degree between the maximum circumferential stress ($\sigma(\theta)_{\max}$) and the pre-existing flaw. The anticlockwise is set as the positive direction of γ . The maximum circumferential stress ($\sigma(\theta)_{\max}$) of every flaw tip in every specimen is listed in Table 2.

From Park and Bobet (2010), Wong and Einstein (2009) and the testing results in this study, it can be seen that most of the coalescence cracks linked from or near flaw tips. In this study we described the link lines between two flaw tips at the bridge area as the potential coalescence paths (Fig.8). Fig. 8 shows that there are more potential coalescence paths in specimens containing two aligned X-type flaws than those containing two parallel single flaws. The question remaining is that in these potential coalescence paths which one will be the real one. From experimental results in this study we concluded 2 characteristics for the crack coalescence of the aligned X-type flaws under uniaxial compression:

Characteristics 1. The cracks tend to coalesce by cracks emanating from flaw tips along a potential path that is parallel to the maximum compressive stress direction.

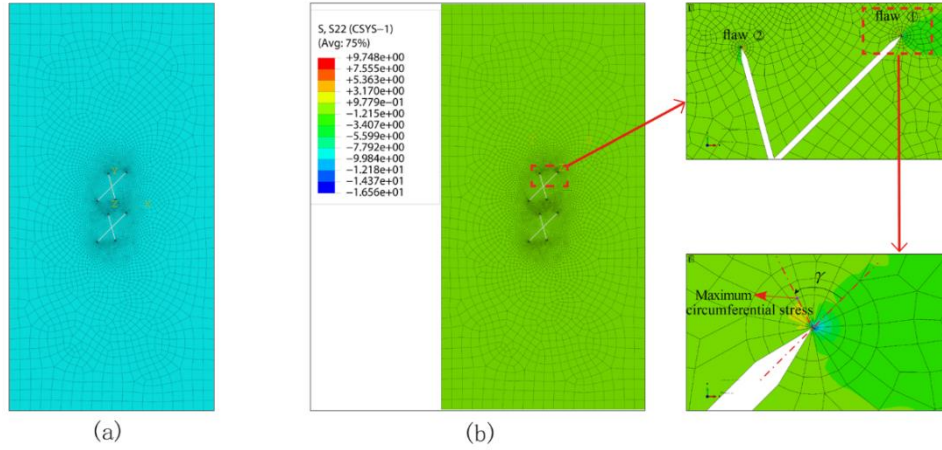


Fig. 7 Simulation of Specimen C5: (a) the computation model and (b) the circumferential stress (σ_{θ}) field

Table 2 Maximum circumferential stresses ($\sigma(\theta)_{\max}$) of flaw tips from computation

| No. | Maximum circumferential stresses ($\sigma(\theta)_{\max}$) of flaw tips (MPa) | | | | | | | | | | | | | | | |
|-----|---|------------------------------|----------------|------------------------------|----------------|------------------------------|----------------|------------------------------|----------------|------------------------------|----------------|------------------------------|----------------|------------------------------|----------------|------------------------------|
| | flaw ① | | flaw ② | | | | flaw ③ | | | | flaw ④ | | | | | |
| | outer flaw tip | Position $/\gamma(^{\circ})$ | inner flaw tip | Position $/\gamma(^{\circ})$ | outer flaw tip | Position $/\gamma(^{\circ})$ | inner flaw tip | Position $/\gamma(^{\circ})$ | inner flaw tip | Position $/\gamma(^{\circ})$ | outer flaw tip | Position $/\gamma(^{\circ})$ | inner flaw tip | Position $/\gamma(^{\circ})$ | outer flaw tip | Position $/\gamma(^{\circ})$ |
| C1 | 0.973 | 72.625 | 0.734 | 72.625 | - | - | - | - | 0.735 | 72.625 | 0.970 | 72.625 | - | - | - | - |
| C2 | 0.773 | 72.625 | 0.628 | 72.625 | 0.568 | 51.875 | 0.389 | 51.875 | 0.628 | 72.625 | 0.772 | 72.625 | 0.388 | 51.875 | 0.567 | 51.875 |
| C3 | 0.661 | 72.625 | 0.567 | 72.625 | 0.408 | 10.375 | 0.295 | 10.375 | 0.567 | 72.625 | 0.661 | 72.625 | 0.295 | 10.375 | 0.408 | 10.375 |
| C4 | 0.716 | 72.625 | 0.580 | 72.625 | 0.407 | -10.375 | 0.242 | -10.375 | 0.580 | 72.625 | 0.715 | 72.625 | 0.242 | -10.375 | 0.406 | -10.375 |
| C5 | 0.829 | 72.625 | 0.614 | 72.625 | 0.493 | -51.875 | 0.231 | -31.125 | 0.613 | 72.625 | 0.828 | 72.625 | 0.231 | -31.125 | 0.493 | -51.875 |
| C6 | 0.942 | 72.625 | 0.667 | 72.625 | 0.621 | -62.250 | 0.264 | -51.875 | 0.666 | 72.625 | 0.941 | 72.625 | 0.264 | -51.875 | 0.620 | -62.25 |
| C7 | 1.002 | 72.625 | 0.705 | 72.625 | 0.717 | -83.000 | 0.354 | -72.625 | 0.705 | 72.625 | 1.026 | 72.625 | 0.354 | -72.625 | 0.717 | -83.000 |
| C8 | 1.071 | 72.625 | 0.722 | 72.625 | 0.678 | -93.375 | 0.455 | -83.000 | 0.721 | 72.625 | 1.069 | 72.625 | 0.455 | -83.000 | 0.678 | -93.375 |
| C9 | 1.076 | 72.625 | 0.729 | 72.625 | 0.494 | -103.750 | 0.438 | -103.750 | 0.728 | 72.625 | 1.074 | 72.625 | 0.437 | -103.750 | 0.494 | -103.750 |
| C10 | 1.056 | 72.625 | 0.734 | 72.625 | 0.288 | 103.750 | 0.279 | 103.750 | 0.734 | 72.625 | 1.054 | 72.625 | 0.279 | 103.750 | 0.288 | 103.750 |
| C11 | 1.028 | 72.625 | 0.741 | 72.625 | 0.219 | 83.000 | 0.240 | 83.000 | 0.741 | 72.625 | 1.027 | 72.625 | 0.240 | 83.000 | 0.219 | 83.000 |
| C12 | 0.999 | 72.625 | 0.742 | 72.625 | 0.085 | 41.500 | 0.081 | 41.500 | 0.742 | 72.625 | 0.997 | 72.625 | 0.081 | 41.500 | 0.085 | 41.500 |

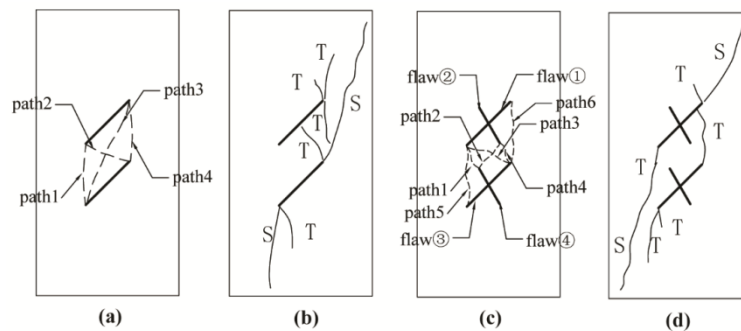


Fig. 8 Comparison between the potential coalescence paths and the real coalescence cracks of testing conditions C1 and C6. (a) The potential coalescence paths of C1, (b) The real coalescence cracks of C1, (c) The potential coalescence paths of C6 and (d) The real coalescence cracks of C6

Characteristics 2. The cracks are more likely to coalesce along the coalescence path linked by flaw tips with greater maximum circumferential stress ($\sigma(\theta)_{\max}$) if there are several potential coalescence paths almost parallel to the

maximum compressive stress direction.

Fig. 8 provides the potential coalescence paths and real coalescence cracks of testing conditions C1 and C6. In order to show the potential coalescence paths clearly, the

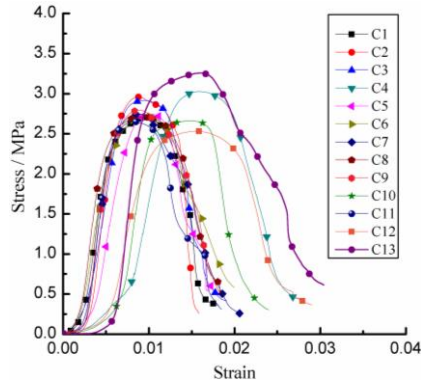


Fig. 9 The stress-strain curves of tested specimens

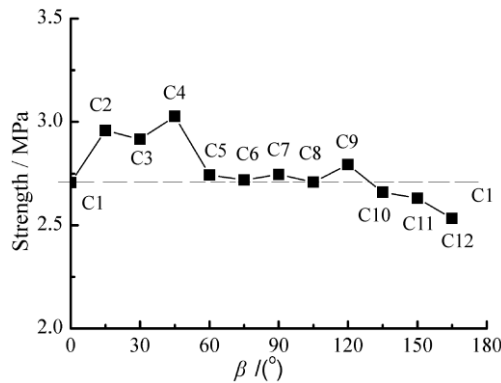


Fig. 10 The peak strengths of specimens C1 to C12 The dash line is the strength of specimen containing two single flaws (the testing condition C1).

Table 3 The peak strengths of specimens under uniaxial compression testing condition

| No. | Strength/MPa |
|-----|--------------|
| C1 | 2.706 |
| C2 | 2.958 |
| C3 | 2.916 |
| C4 | 3.027 |
| C5 | 2.743 |
| C6 | 2.719 |
| C7 | 2.746 |
| C8 | 2.708 |
| C9 | 2.793 |
| C10 | 2.660 |
| C11 | 2.651 |
| C12 | 2.532 |

flaws, the potential coalescence paths and real coalescence cracks in Fig.8 are magnified in the schematic diagram. Fig. 8(a) shows that there are 4 potential coalescence paths at the rock bridge area of C1. Fig. 8(c) illustrates that there are 6 potential coalescence paths at the rock bridge area of C6. It is very clear that there are more potential coalescence paths in specimens containing two aligned X-type flaws than in those containing two parallel single flaws.

The testing condition C6 is taken as an example to explain the cracks coalescence characteristics in specimens

with two aligned X-type flaws (see Fig. 8(c) and 8(d)). In C6 the coalescence crack initiating from one primary flaw passes the secondary flaw tip and coalesces with the crack initiated from another primary flaw. From Fig. 8(c) one can see that there are 6 potential paths at the bridge area. Paths 1, 4, 5 and 6 are almost parallel to the maximum compressive stress direction (vertical loading direction). Paths 1, 4, 5 and 6 are more consistent with the direction of the maximum compressive stress than paths 2 and 3. As described in the Characteristics 1, paths 1, 4, 5 and 6 have a larger possibility to become the coalescence cracks than paths 2 and 3. Then we discuss the coalescence possibility among paths 1, 4, 5 and 6. Path 5 is the link between the inner tip of flaw ① and outer tip of flaw ③. Path 1 is the link between the inner tip of flaw ① and inner tip of flaw ④. From Table 2 it can be seen that the maximum circumferential stress of flaw ③ outer tip (0.941MPa) is larger than that of flaw ④ inner tip (0.264MPa). For the Characteristics 2, the cracks more possibly coalesce along path 5 than path 1. Path 6 is the link between the outer tip of flaw ① and inner tip of flaw ③, and path 4 is the link between the inner tips of flaw ② and flaw ③. From Table 2 it can be seen that the maximum circumferential stress of flaw ① outer tip (0.942MPa) is larger than that of flaw ② inner tip (0.264MPa). Again as mentioned in the Characteristics 2 above, the coalescence crack is more possibly formed along path 6 than path 4. Considering paths 5 and 6, from Table 2 we see that the maximum circumferential stress of flaw ① outer tip (0.942MPa) is larger than that of flaw ③ outer tip (0.941MPa). Therefore, the coalescence crack is more likely to be formed along path 6 than path 5. From the experimental results we observe the coalescence cracks occurred along path 6, which is consistent with Characteristics 1 and 2.

From Figs. 5 and 6, one can see the crack coalescences at the bridge areas in other specimens are also consistent with the two characteristics discussed above.

3.2 Strengths of rock-like material specimens containing two aligned X-type flaws under uniaxial compression

The failure modes of specimens containing two parallel single flaws and two aligned X-type flaws under uniaxial compression are shown in Figs 5 and 6. The stress-strain curves of all tested conditions and peak strengths of specimens C1 to C12 are plotted in Figs. 9 and 10 and listed in Table 3.

From Figs. 9 and 10 and Table 3, it can be seen that 8 out of 11 specimens containing two aligned X-type flaws have higher peak strength than that of the specimens containing two single flaws, and 3 out of 11 testing specimens containing two aligned X-type flaws have lower strength than that of the specimens containing two single flaws. These results show that the secondary flaws either enhance or reduce the strength of the rock-like material under uniaxial compression. In the following text we try to explain the influence of secondary flaw to the specimen strength through analyzing the flaw tips stresses and propagation tendencies.

Based on the experimental results known, the wing crack initiation is associated with the maximum circumferential stress($\sigma(\theta)_{max}$), and the shear crack initiation

Table 4 Maximum shear stresses of flaw tips

| No. | Maximum shear stresses ($ \tau(\theta)_{\max} $) of flaw tips / MPa | | | | | | | | | | | | | | | |
|-----|---|--------------------------------------|-------------------|--------------------------------------|-------------------|--------------------------------------|-------------------|--------------------------------------|-------------------|--------------------------------------|-------------------|--------------------------------------|-------------------|--------------------------------------|-------------------|--------------------------------------|
| | flaw ① | | flaw ② | | flaw ③ | | flaw ④ | | flaw ③ | | flaw ④ | | flaw ③ | | flaw ④ | |
| | outer flaw tip | Position $\angle\gamma(^{\circ})$ | inner flaw tip | Position $\angle\gamma(^{\circ})$ | outer flaw tip | Position $\angle\gamma(^{\circ})$ | inner flaw tip | Position $\angle\gamma(^{\circ})$ | inner flaw tip | Position $\angle\gamma(^{\circ})$ | outer flaw tip | Position $\angle\gamma(^{\circ})$ | inner flaw tip | Position $\angle\gamma(^{\circ})$ | outer flaw tip | Position $\angle\gamma(^{\circ})$ |
| C1 | 1.268 | 20.75 | 1.123 | 10.375 | - | - | - | - | 1.122 | 10.375 | 1.266 | 20.75 | - | - | - | - |
| C2 | 1.203 | 10.375 | 1.120 | 0.000 | 0.327 | 0.000 | 0.224 | 0 | 1.120 | 0 | 1.202 | 10.375 | 0.224 | 0 | 0.326 | 0 |
| C3 | 1.159 | 10.375 | 1.104 | 0.000 | 0.269 | -41.5 | 0.184 | -41.5 | 1.104 | 0 | 1.159 | 10.375 | 0.184 | -41.5 | 0.269 | -41.500 |
| C4 | 1.178 | 10.375 | 1.100 | 0.000 | 0.438 | 31.125 | 0.167 | 41.5 | 1.100 | 0 | 1.178 | 10.375 | 0.167 | 41.5 | 0.435 | 41.500 |
| C5 | 1.220 | 10.375 | 1.096 | 0.000 | 0.613 | 20.75 | 0.267 | 20.75 | 1.096 | 0 | 1.219 | 10.375 | 0.266 | 20.75 | 0.612 | 20.750 |
| C6 | 1.250 | 10.375 | 1.095 | 0.000 | 0.749 | 0.000 | 0.412 | 10.375 | 1.095 | 0 | 1.249 | 10.375 | 0.412 | 10.375 | 0.749 | 0 |
| C7 | 1.259 | 20.75 | 1.078 | 0.000 | 0.840 | -20.75 | 0.559 | 0.000 | 1.078 | 0 | 1.252 | 10.375 | 0.559 | 0 | 0.840 | -20.750 |
| C8 | 1.245 | 20.75 | 1.037 | 0.000 | 0.881 | -31.125 | 0.683 | -20.750 | 1.037 | 0 | 1.244 | 20.75 | 0.683 | -20.75 | 0.881 | -31.125 |
| C9 | 1.218 | 20.75 | 0.993 | 10.375 | 0.837 | -41.5 | 0.736 | -41.500 | 0.993 | 10.375 | 1.217 | 20.75 | 0.736 | -41.5 | 0.837 | -41.500 |
| C10 | 1.198 | 20.75 | 0.977 | 10.375 | 0.768 | 41.5 | 0.703 | 51.875 | 0.976 | 10.375 | 1.197 | 20.75 | 0.703 | 51.875 | 0.767 | 41.500 |
| C11 | 1.208 | 20.75 | 1.005 | 10.375 | 0.740 | 20.75 | 0.699 | 31.125 | 1.005 | 10.375 | 1.207 | 20.75 | 0.698 | 31.125 | 0.740 | 20.750 |
| C12 | 1.249 | 20.75 | 1.078 | 10.375 | 0.674 | -10.375 | 0.605 | 0.000 | 1.078 | 10.375 | 1.248 | 20.75 | 0.605 | 0 | 0.673 | -10.375 |

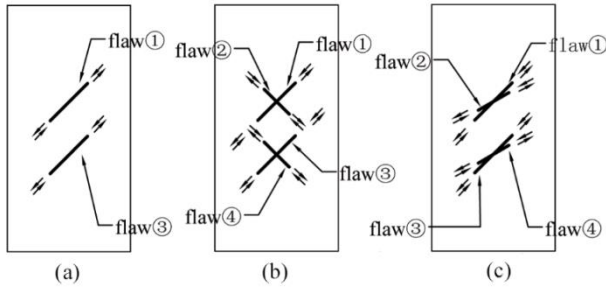


Fig. 11 The shear cracks propagation tendencies of some specimens. (a), (b) and (c) denote testing conditions C1, C7 and C12. The arrows denote the shear cracks propagation tendency

with the maximum absolute shear stress ($|\tau(\theta)_{\max}|$) (Bobet 2000). As the specimens with flaws fail from flaw tips initiation to cracks propagation, so the two maximum stresses are also significant factors to influence the specimens' strengths. The maximum circumferential stresses ($\sigma(\theta)_{\max}$) of flaw tips have been listed in Table 2. The flaw tips maximum shear stresses $|\tau(\theta)_{\max}|$ (absolute value) are listed in Table 4.

We see that the rock-like material specimens under uniaxial compression fail mostly with shear crack (Yin *et al.* 2014, Wong and Einstein 2009). Therefore, it is believed that influence the shear crack propagation tendency may affect the specimens' strengths. The shear cracks propagation tendency of specimens C1, C7 and C12 are plotted in Fig. 11 to analyze the influence of secondary flaws on specimen strengths as examples.

From Tables 2 and 4 one can see the $\sigma(\theta)_{\max}$ and $|\tau(\theta)_{\max}|$ of testing conditions C2, C3, C4, C5, C6 are lower than those of the testing condition C1. This is the important reason that the strengths of C2, C3, C4, C5, C6 are higher than that of C1.

From Fig. 11(b) it can be seen that the shear crack propagation tendencies of primary flaws ① and ③ are

left-lateral, but the shear crack propagation tendencies of secondary flaws ② and ④ are right-lateral. The right-lateral shear crack propagation tendencies of secondary flaws ② and ④ may delay the shear crack propagation of flaws ① and ③, which enhances the strength of specimens with X-type flaws under this situation. So although $\sigma(\theta)_{\max}$ of the testing condition C7 are a little higher than those of C1, the strength of C7 is higher than that of C1. The flaws geometry of C7, C8 and C9 are almost in the same situation. So although $\sigma(\theta)_{\max}$ of C8 and C9 are higher than those of C1, the strengths of C8 and C9 are higher than that of C1.

From Fig. 11(c) it can be seen that the shear crack propagation tendencies of the C12 primary flaws ① and ③ as well as secondary flaws ② and ④ are all left-lateral. The left-lateral shear crack propagation tendencies of secondary flaws ② and ④ may enhance the shear crack propagation of the same left-lateral flaws ① and ③. Thus leads the strength of C12 is lower than that of C1. The testing condition C11 is almost in the same situation with C12, so the strength of C11 is lower than that of C1. The secondary flaws ② and ④ of C10 are vertical to the loading direction. Its shear crack propagation has little influence on the primary flaws shear crack propagation. So C10 has almost same strength with that of C1.

4. Conclusions

Uniaxial compression tests were conducted on rock-like material samples containing two aligned X-type flaws and two single parallel flaws. The conclusions from this work can be drawn as follows.

- The crack coalescence occurs by emanating cracks from flaw tips along a potential path that is parallel to the

maximum compressive stress direction.

- The cracks are more likely to coalesce along the coalescence path linked by flaw tips with greater maximum circumferential stress if there are several potential coalescence paths almost parallel to the maximum compressive stress direction.

- Some of the specimens containing two aligned X-type flaws have higher strengths than that of the specimen containing two single parallel flaws. One reason is that the flaw tips maximum circumferential stress and maximum shear stress of some specimens with two aligned X-type flaws are lower than those of specimens containing two single parallel flaws. The other reason is that the shear crack propagation tendencies of some secondary flaws may delay that of the main flaws.

Acknowledgements

This paper is funded by National Natural Science Foundation of China (NO. 51879151, 51379114), and partial support from the Chinese government plan on the Recruitment of Global Young Talents. K.X. acknowledges support by the Natural Sciences and Engineering Research Council of Canada (NSERC) through the Discovery Grant # 72031326.

References

- Al-Shayea, N. A. (2005), "Crack propagation trajectories for rocks under mixed mode I-II fracture", *Eng. Geol.*, **81**(1), 84-97.
- Bobet, A. (2000), "The initiation of secondary cracks in compression", *Eng. Fract. Mech.*, **66**(2), 187-219.
- Bobet, A. and Einstein, H.H. (1998), "Fracture coalescence in rock-type materials under uniaxial and biaxial compression", *Int. J. Rock Mech. Min. Sci.*, **35**(7), 863-888.
- Cao, P., Liu, T., Pu, C. and Lin, H. (2015), "Crack propagation and coalescence of brittle rock-like specimens with pre-existing cracks in compression", *Eng. Geol.*, **187**, 113-121.
- Chen, Y., Ni, J., Shao, W., Zhou, Y., Javadi, A. and Azzam, R. (2012), "Coalescence of fractures under uni-axial compression and fatigue loading", *Rock Mech. Rock Eng.*, **45**(2), 241-249.
- Cheng, H., Zhou, X., Zhu, J. and Qian, Q. (2016), "The effects of crack openings on crack initiation, propagation and coalescence behavior in rock-like materials under uniaxial compression", *Rock Mech. Rock Eng.*, **49**(9), 1-14.
- Feng, P., Dai, F., Liu, Y., Xu, N.W. and Fan, P.X. (2017), "Effects of coupled static and dynamic strain rates on mechanical behaviors of rock-like specimens containing pre-existing fissures under uniaxial compression", *Can. Geotech. J.*, **55**(5), 640-652.
- Griffith, A.A. (1921), "The phenomena of rupture and flow in solids", *Phil. Trans. R. Soc. Lond. A*, **221**(582-593), 163-198.
- Haeri, H., Shahriar, K., Marji, M.F. and Moarefvand, P. (2014), "Experimental and numerical study of crack propagation and coalescence in pre-cracked rock-like disks", *Int. J. Rock Mech. Min. Sci.*, **67**, 20-28.
- Hoek, E. and Bieniawski, Z. (1965), "Brittle fracture propagation in rock under compression", *Int. J. Fract. Mech.*, **1**(3), 137-155.
- Huang, J., Chen, G., Zhao, Y. and Wang, R. (1990), "An experimental study of the strain field development prior to failure of a marble plate under compression", *Tectonophysics*, **175**(1), 269-284.
- Lajtai, E.Z. (1974), "Brittle fracture in compression", *Int. J. Fract.*, **10**(4), 525-536.
- Li, S., Wang, J., Chen, W., Li, L. and Zhang, Q. (2016), "Study on mechanism of macro failure and micro fracture of local nearly horizontal stratum in super-large section and deep buried tunnel", *Geomech. Eng.*, **11**(2), 253-267.
- Li, Y.P., Chen, L.Z. and Wang, Y.H. (2005), "Experimental research on pre-cracked marble under compression", *Int. J. Solids Struct.*, **42**(9), 2505-2516.
- Li, Y., Zhou, H., Zhang, L., Zhu, W., Li, S. and Liu, J. (2016), "Experimental and numerical investigations on mechanical property and reinforcement effect of bolted jointed rock mass", *Construct. Build. Mater.*, **126**, 843-856.
- Liu, Y. and Dai, F. (2018), "A damage constitutive model for intermittent jointed rocks under cyclic uniaxial compression", *Int. J. Rock Mech. Min. Sci.*, **103**, 289-301.
- Liu, Y., Dai, F., Dong, L., Xu, N.W. and Feng, P. (2018), "Experimental investigation on the fatigue mechanical properties of intermittently jointed rock models under cyclic uniaxial compression with different loading parameters", *Rock Mech. Rock Eng.*, **51**(1), 47-68.
- Liu, Y., Dai, F., Fan, P., Xu, N.W. and Dong, L. (2017a), "Experimental investigation of the influence of joint geometric configurations on the mechanical properties of intermittent jointed rock models under cyclic uniaxial compression", *Rock Mech. Rock Eng.*, **50**(6), 1453-1471.
- Liu, Y., Dai, F., Zhao, T. and Xu, N.W. (2017c), "Numerical investigation of the dynamic properties of intermittent jointed rock models subjected to cyclic uniaxial compression", *Rock Mech. Rock Eng.*, **50**(1), 89-112.
- Park, C.H. and Bobet, A. (2009), "Crack coalescence in specimens with open and closed flaws: A comparison", *Int. J. Rock Mech. Min. Sci.*, **46**(5), 819-829.
- Park, C.H. and Bobet, A. (2010), "Crack initiation, propagation and coalescence from frictional flaws in uniaxial compression", *Eng. Fract. Mech.*, **77**(14), 2727-2748.
- Pu, C.Z. and Cao, P. (2012), "Failure characteristics and its influencing factors of rock-like material with multi-fissures under uniaxial compression", *Trans. Nonf. Met. Soc. Chin.*, **22**(1), 185-191.
- Sagong, M., Park, D., Yoo, J. and Lee, J.S. (2011), "Experimental and numerical analyses of an opening in a jointed rock mass under biaxial compression", *Int. J. Rock Mech. Min. Sci.*, **48**(7), 1055-1067.
- Sagong, M. and Bobet, A. (2002), "Coalescence of multiple flaws in a rock-model material in uniaxial compression", *Int. J. Rock Mech. Min. Sci.*, **39**(2), 229-241.
- Sahouryeh, E., Dyskin, A. and Germanovich, L. (2002), "Crack growth under biaxial compression", *Eng. Fract. Mech.*, **69**(18), 2187-2198.
- Sharafisafa, M. and Nazem, M. (2014), "Application of the distinct element method and the extended finite element method in modelling cracks and coalescence in brittle materials", *Comput. Mater. Sci.*, **91**, 102-121.
- Shen, B., Stephansson, O., Einstein, H.H. and Ghahreman, B. (1995), "Coalescence of fractures under shear stresses in experiments", *J. Geophys. Res. Solid Earth*, **100**(6), 5975-5990.
- Tang, C.A., Lin, P., Wong, R.H.C. and Chau, K.T. (2001), "Analysis of crack coalescence in rock-like materials containing three flaws-part II: Numerical approach", *Int. J. Rock Mech. Min. Sci.*, **38**(7), 925-939.
- Wei, M., Dai, F., Xu, N. and Zhao, T. (2016), "Stress intensity factors and fracture process zones of ISRM-suggested chevron notched specimens for mode I fracture toughness testing of rocks", *Eng. Fract. Mech.*, **168**, 174-189.
- Wong, L.N.Y. and Einstein, H.H. (2009), "Crack coalescence in molded gypsum and Carrara marble: Part I. Macroscopic

- observations and interpretation”, *Rock Mech. Rock Eng.*, **42**(3), 475-511.
- Wong, L.N.Y. and Einstein, H.H. (2009), “Crack coalescence in molded gypsum and Carrara marble: Part 2-microscopic observations and interpretation”, *Rock Mech. Rock Eng.*, **42**(3), 513-545.
- Wong, L.N.Y. and Einstein, H.H. (2009), “Systematic evaluation of cracking behavior in specimens containing single flaws under uniaxial compression”, *Int. J. Rock Mech. Min. Sci.*, **46**(2), 239-249.
- Wong, R.H. and Chau, K. (1998), “Crack coalescence in a rock-like material containing two cracks”, *Int. J. Rock Mech. Min. Sci.*, **35**(2), 147-164.
- Wong, R., Chau, K., Tang, C. and Lin, P. (2001), “Analysis of crack coalescence in rock-like materials containing three flaws-part I: Experimental approach”, *Int. J. Rock Mech. Min. Sci.*, **38**(7), 909-924.
- Yang, S.Q. (2011), “Crack coalescence behavior of brittle sandstone samples containing two coplanar fissures in the process of deformation failure”, *Eng. Fract. Mech.*, **78**(17), 3059-3081.
- Yin, P., Wong, R. and Chau, K. (2014), “Coalescence of two parallel pre-existing surface cracks in granite”, *Int. J. Rock Mech. Min. Sci.*, **68**, 66-84.
- Zhang, B., Li, S., Xia, K., Yang, X., Zhang, D., Wang, S. and Zhu, J. (2016), “Reinforcement of rock mass with cross-flaws using rock bolt”, *Tunn. Undergr. Sp. Technol.*, **51**, 346-353.
- Zhou, X.P., Chen, H. and Feng, Y.F. (2014), “An experimental study of crack coalescence behaviour in rock-like materials containing multiple flaws under uniaxial compression”, *Rock Mech. Rock Eng.*, **47**(6), 1961-1986.
- Zhou, X.P., Wang, Y.T., Zhang, J.Z. and Liu, F.N. (2018), “Fracturing behavior study of three-flawed specimens by uniaxial compression and 3D digital image correlation: Sensitivity to brittleness”, *Rock Mech. Rock Eng.*, 1-28.

GC

Nomenclature

| | |
|--------------------------|--|
| α | the angle between the primary flaws (i.e. flaws ① or ③) and the horizontal direction |
| β | the angle between the primary and secondary flaws |
| $L13$ | the length of primary flaws |
| $L24$ | the length of secondary flaws |
| $C1-C12$ | testing conditions |
| σ_{θ} | the circumferential stress |
| $\sigma(\theta)_{max}$ | the maximum circumferential stress |
| $ \tau(\theta r)_{max} $ | the maximum shear stress (absolute value) |
| T | tensile cracks |
| S | shear cracks |